Neutralizing antibody and soluble ACE2 inhibition of a replication-competent VSV-SARS-CoV-2 and a clinical isolate of SARS-CoV-2.

James Brett Case[1]*, Paul W. Rothlauf[2,6]*, Rita E. Chen[1,3], Zhuoming Liu[2], Haiyan Zhao[4], Arthur S. Kim[1,3], Louis-Marie Bloyet[2], Qiru Zeng[2], Stephen Tahan[2], Lindsay Droit[2], Ma. Xenia G. Ilagan[4], Michael A. Tartell[2,6], Gaya Amarasinghe[2,3,4], Jeffrey P. Henderson[1], Shane Miersch[7], Mart Ustav[7], Sachdev Sidhu[7], Herbert W. Virgin[8], David Wang[2], Siyuan Ding[2], Davide Corti[9], Elitza S. Theel[10], Daved H. Fremont[2,3,4,5], Michael S. Diamond[1,2,4,5]‡, and Sean P.J. Whelan[2]‡,

Department of Medicine[1], Molecular Microbiology[2], Pathology & Immunology[3], Biochemistry & Molecular Biophysics[4] and The Andrew M. and Jane M. Bursky Center for Human Immunology & Immunotherapy Programs[5], Washington University School of Medicine, St. Louis, MO, USA. [6]Program in Virology, Harvard Medical School, Boston, MA, USA. [7]The Donnelly Centre, University of Toronto, Toronto, Canada. [8]Vir Biotechnology, San Francisco, CA, USA. [9]Humabs BioMed SA, a subsidiary of Vir Biotechnology, Inc., CH-6500, Bellinzona, Switzerland. [10]Division of Clinical Microbiology, Department of Laboratory Medicine and Pathology, Mayo Clinic, Rochester, MN, USA

* Equal contributors

‡ **Corresponding authors:** Sean P.J. Whelan Ph.D., spjwhelan@wustl.edu and Michael S. Diamond, M.D., Ph.D., diamond@wusm.wustl.edu;

Figures: 5

ABSTRACT

Antibody-based interventions against SARS-CoV-2 could limit morbidity, mortality, and possibly disrupt epidemic transmission. An anticipated correlate of such countermeasures is the level of neutralizing antibodies against the SARS-CoV-2 spike protein, yet there is no consensus as to which assay should be used for such measurements. Using an infectious molecular clone of vesicular stomatitis virus (VSV) that expresses eGFP as a marker of infection, we replaced the glycoprotein gene (G) with the spike protein of SARS-CoV-2 (VSV-eGFP-SARS-CoV-2) and developed a high-throughput imaging-based neutralization assay at biosafety level 2. We also developed a focus reduction neutralization test with a clinical isolate of SARS-CoV-2 at biosafety level 3. We compared the neutralizing activities of monoclonal and polyclonal antibody preparations, as well as ACE2-Fc soluble decoy protein in both assays and find an exceptionally high degree of concordance. The two assays will help define correlates of protection for antibody-based countermeasures including therapeutic antibodies, immune γ-globulin or plasma preparations, and vaccines against SARS-CoV-2. Replication-competent VSV-eGFP-SARS-CoV-2 provides a rapid assay for testing inhibitors of SARS-CoV-2 mediated entry that can be performed in 7.5 hours under reduced biosafety containment.

INTRODUCTION

Severe acute respiratory syndrome coronavirus 2 (SARS-CoV-2) is a positive-sense, single-stranded, enveloped RNA virus that was first isolated in Wuhan, China in December, 2019 from a cluster of acute respiratory illness cases (Guan et al., 2020). SARS-CoV-2 is the etiologic agent of coronavirus disease 2019 (COVID-19), which as of May 16, 2020 has more than 4.5 million confirmed cases causing 309,000 deaths. Virtually all countries and territories have been affected, with major epidemics in Central China, Italy, Spain, France, Iran, Russia, the United Kingdom, and the United States. SARS-CoV-2 is thought to be of zoonotic origin and is closely related to the original SARS-CoV (Zhang et al., 2020; Zhou et al., 2020). Most cases are spread by direct human-to-human transmission, with community transmission occurring from both symptomatic and asymptomatic individuals (Bai et al., 2020). This has resulted in a global pandemic with severe economic, political, and social consequences. The development, characterization, and deployment of an effective vaccine or antibody prophylaxis or treatment against SARS-CoV-2 could prevent morbidity and mortality and curtail its epidemic spread.

The viral spike protein (S) mediates all steps of coronavirus entry into target cells including receptor binding and membrane fusion (Tortorici and Veesler, 2019). During viral biogenesis the S protein undergoes furin-dependent proteolytic processing as it transits through the trans-Golgi network and is cleaved into S1 and S2 subunits that function in receptor binding and membrane fusion, respectively (Walls et al., 2020). Angiotensin-converting enzyme 2 (ACE2) serves as a cell surface receptor (Letko et al., 2020; Wrapp et al., 2020) for SARS-CoV-2, and productive infection is facilitated by additional processing of S2 by the host cell serine protease TMPRSS2 (Hoffmann et al., 2020).

Laboratory studies of SARS-CoV-2 require biosafety level 3 (BSL3) containment with positive-pressure respirators. Single-round pseudotyped viruses complemented by expression of the SARS-CoV-2 S protein *in trans* serve as biosafety level 2 (BSL2) surrogates that can facilitate studies of viral entry, and the inhibition of infection by neutralizing antibodies and other inhibitors

(Hoffmann et al., 2020; Lei et al., 2020; Ou et al., 2020). Such pseudotyping approaches are used routinely by many laboratories for other highly pathogenic coronaviruses including SARS-CoV and MERS-CoV (Fukushi et al., 2006; Fukushi et al., 2005; Giroglou et al., 2004; Kobinger et al., 2007). Viral pseudotyping assays are limited by the need to express the glycoprotein *in trans* and preclude forward genetic studies of the viral envelope protein. Expression of the glycoprotein is often accomplished by plasmid transfection, which requires optimization to minimize batch variation. Assays performed with such pseudotyped viruses rely on relative levels of infectivity as measured by a reporter assay without correlation to an infectious titer. It also is unknown as to how the display of S proteins on a heterologous virus impacts viral entry, antibody recognition, and antibody neutralization compared to infectious coronavirus. This question is important because neutralization assays are used to establish correlates of protection for vaccine and antibody-based countermeasures, and most manufacturers lack access to high-containment laboratories to test antibody responses against highly pathogenic coronaviruses including SARS-CoV-2.

Here, we developed a simple and robust BSL2 assay for evaluating SARS-CoV-2 entry and its inhibition by antibodies. We engineered an infectious molecular clone of vesicular stomatitis virus (VSV) to encode the SARS-CoV-2 S protein in place of the native envelope glycoprotein (G) and rescued an autonomously replication-competent virus bearing the spike. Through passage of VSV-eGFP-SARS-CoV-2, we selected a gain-of-function mutation in S that allowed more efficient viral propagation yielding titers of > 1 x 10^8 plaque-forming units (PFU)/ml. We characterized this variant with respect to inhibition by soluble human ACE2-Fc and monoclonal and polyclonal antibodies from humans and compared those results to neutralization tests with a clinical isolate of SARS-CoV-2. These studies demonstrate that a recombinant VSV expressing SARS-CoV-2 S behaves analogously to a clinical isolate of SARS-CoV-2, providing a useful high-throughput BSL2 assay for studying antibody neutralization or inhibition of viral spike-mediated entry.

RESULTS

A replication-competent, infectious VSV chimera with SARS-CoV-2 S protein. To generate a replication-competent virus to study entry and neutralization of SARS-CoV-2 at BSL2, we engineered an infectious molecular clone of VSV by replacing the endogenous glycoprotein (G) with SARS-CoV-2 S (**Fig 1A**). SARS-CoV-2 S protein contains an endoplasmic reticulum (ER) retention sequence in the cytoplasmic tail (KxHxx-COOH) because virion assembly occurs in ER-Golgi intermediate compartments (Lontok et al., 2004; McBride et al., 2007; Ruch and Machamer, 2012). We preemptively altered that sequence to AxAxx to facilitate retargeting of S to the plasma membrane, the site of VSV assembly. Using established approaches (**Fig S1A**) (Whelan et al., 1995), we recovered infectious VSV-eGFP-SARS-CoV-2-S_{AA} as determined by expression of the virus-encoded eGFP reporter (**Fig 1A,** *right panel*). VSV-eGFP-SARS-CoV-2-S_{AA} propagation was inefficient on Vero CCL81 cells. This result prompted us to test additional modifications of the cytoplasmic tail of S, which were also defective in autonomous amplification (**Fig S1B**). To overcome this limitation, we used a forward genetic approach to isolate an adaptive variant of VSV-eGFP-SARS-CoV-2-S_{AA} **(Fig S1C**). Repeated passage and plaque isolation on Vero CCL81 cells led to the emergence of a virus that contained a cysteine to stop mutation at residue 1253 (TGC to TGA at nucleotide 3759), which truncates the cytoplasmic tail of SARS-CoV-2 S by 21 residues (**Fig 1A**). We confirmed that this was the only mutation in the viral genome by next generation sequencing (Supplemental Data). Comparison of plaque morphology of VSV-eGFP-SARS-CoV-2-$S_{\Delta 21}$ and VSV-eGFP-SARS-CoV-2-S_{AA} on three Vero cell subtypes and an additional rhesus monkey cell line (MA104) demonstrates that the selected variant spreads more efficiently (**Fig 1B**). Screening of a larger panel of cell types (**Fig 1C**) identified MA104 and Vero E6 cells as supporting the highest levels of virus production. Ectopic expression of TMPRSS2 led to a further ~10-fold increase in viral titer and a larger plaque size (**Fig 1D**).

SARS-CoV-2-$S_{\Delta 21}$ is incorporated into infectious VSV particles. To confirm incorporation of SARS-CoV-2 S into particles, we first amplified the virus in the presence of VSV

G to allow infection of cell types independently of the S protein. The VSV G *trans*-complemented VSV-SARS-CoV-2-$S_{\Delta 21}$ efficiently infects HEK293T cells, which then serve as a source of production of virus particles containing SARS-CoV-2 S protein. Western blotting of supernatants with CR3022, a cross-reactive anti-S monoclonal antibody (mAb) (ter Meulen et al., 2006; Yuan et al., 2020), established the presence of $S_{\Delta 21}$ in VSV-SARS-CoV-2-$S_{\Delta 21}$ particles but not in the parental VSV (**Fig 1E**). The protein detected migrated at ~100 kilodaltons, a band that corresponds to the cleaved S1 subunit of the glycoprotein (Watanabe et al., 2020). To examine whether the $S_{\Delta 21}$ incorporated into VSV particles is processed to S1 and S2, we performed [^{35}S] cysteine-methionine metabolic labeling in BSRT7 cells, which support robust VSV replication, and analyzed released particles by SDS-PAGE and phosphorimaging. In addition to the VSV structural proteins (N, P, M and L), two additional bands were observed for VSV-SARS-CoV-2-$S_{\Delta 21}$ that correspond in size to glycosylated S1 (107 kDa) and $S2_{\Delta 21}$ (85 kDa) (**Fig 1F**). Negative-stain electron microscopy of sucrose-gradient purified virus particles revealed that the membrane protein projecting from VSV-SARS-CoV-2-$S_{\Delta 21}$ is larger than observed on wild-type VSV particles (**Fig 1G**), which reflects the larger size of the coronavirus spike.

A high-throughput focus-forming assay with a clinical isolate of SARS-CoV-2. VSV-SARS-CoV-2-$S_{\Delta 21}$ has several advantages for detection and measuring of neutralizing antibodies, including lower biosafety containment level, ease of production and use, and rapid reporter gene readout. Nonetheless, the difference in virus morphology (spherical CoV versus bullet-shaped VSV) and possible effects on the conformational display of S on the virion surface, raise questions as to whether the accessibility of epitopes and stoichiometry of antibody neutralization is similar to authentic SARS-CoV-2. A direct comparison with a clinical isolate of SARS-CoV-2 is necessary to establish the utility of VSV-SARS-CoV-2-$S_{\Delta 21}$ for assays of viral entry and antibody neutralization.

We designed a high-throughput assay for titrating SARS-CoV-2 that could be applied to multiple cell substrates. Instead of using a plaque assay, which relies on the capacity for a virus

to cause cell death, which can vary across cell types, we developed a focus-forming assay (FFA) and viral antigen detection as a measure of infectivity. We propagated SARS-CoV-2 in four different producer cell types (Vero CCL81, Vero E6, Vero-furin, and MA104 cells) and then measured the number and size of foci after staining recipient cells with an anti-S mAb. With SARS-CoV-2 stocks generated from each producer cell type, we observed distinct foci across recipient cell substrates at approximately 30 h post-inoculation (**Fig 2A**). We consistently observed the highest viral titers and largest foci sizes with Vero-furin and MA104 cells (**Fig 2B-C**). However, the larger foci were more difficult to enumerate on an automated Immunospot reader and required additional manual quality control analysis. Because of this, we used Vero E6 cells for our rapid focus-reduction neutralization tests (FRNT) in subsequent experiments.

A high-throughput, eGFP-based neutralization assay for VSV-SARS-CoV-2-$S_{\Delta 21}$. In parallel, we developed a high-throughput method to measure neutralization of VSV-SARS-CoV-2-$S_{\Delta 21}$. As VSV-SARS-CoV-2-$S_{\Delta 21}$ encodes an eGFP reporter and viral gene expression is robust, eGFP-positive cells can be quantified 7.5 h post-infection using a fluorescence microscope with automated counting analysis software. This approach enabled the development of an eGFP-reduction neutralization test (GRNT) (**Fig 2D**).

Neutralization of VSV-SARS-CoV-2-$S_{\Delta 21}$ and SARS-CoV-2 by human antibodies. Members of our group recently identified human mAbs from memory B cells of a SARS-CoV survivor that bind to SARS-CoV-2 S (Pinto et al, 2020). We tested a subset of these (mAbs 304, 306, 309, and 315) for their ability to inhibit VSV-SARS-CoV-2-$S_{\Delta 21}$ and SARS-CoV-2 infections on Vero E6 cells. While three of these mAbs showed poor inhibitory activity, mAb 309 potently neutralized both SARS-CoV-2 and VSV-SARS-CoV-2-$S_{\Delta 21}$ (**Fig 3A-B**) with similar EC_{50} values between the two assays (81 and 67 ng/mL for SARS-CoV-2 and VSV-SARS-CoV-2-$S_{\Delta 21}$, respectively). To broaden the test panel, we evaluated the activity of a panel of mAbs generated as part of a phage display library (Sachev Sidhu, unpublished data) by both FRNT and GRNT. Many of these mAbs exhibited moderate neutralization activities in the EC_{50} range of 100 to 500

ng/mL (**Fig 3C-D**). Nonetheless, we observed the same neutralization trend between VSV-SARS-CoV-2-$S_{\Delta 21}$ and SARS-CoV-2 with highly correlated EC_{50} values (< 2-fold differences).

Neutralization by human ACE2-Fc receptor decoy proteins. Human ACE2 (hACE2) is an entry receptor for both SARS-CoV and SARS-CoV-2 (Letko et al., 2020; Li et al., 2005; Li et al., 2003; Wrapp et al., 2020). As a soluble hACE2-Fc decoy protein has been proposed as a therapeutic for SARS-CoV-2 (Kruse, 2020), in part based on its ability to inhibit SARS-CoV infection in cell culture (Moore et al., 2004), we tested whether hACE2-Fc could inhibit infection of VSV-SARS-CoV-2-$S_{\Delta 21}$ and SARS-CoV-2 using our FRNT and GRNT assays. When pre-mixed with VSV-SARS-CoV-2-$S_{\Delta 21}$ or SARS-CoV-2, hACE2-Fc, but not murine ACE2-Fc (mACE2-Fc), dose-dependently and equivalently inhibited infection of recipient Vero E6 cells (**Fig 3E-F**). As expected, hACE2-Fc did not inhibit infection of wild-type VSV confirming that neutralization was specific to the SARS-CoV-2 S protein (**Fig S2**). We noted a relatively high concentration of hACE2-Fc was required for inhibition with EC_{50} values of 29 and 12.6 µg/ml for VSV-SARS-CoV-2-$S_{\Delta 21}$ and SARS-CoV-2, respectively. Thus, although soluble hACE2-Fc decoy proteins similarly inhibit infection of VSV-SARS-CoV-2-$S_{\Delta 21}$ and SARS-CoV-2, the potency is less than anticipated, which suggests that the receptor-binding domain (RBD) on the S protein on the surface of both viruses may not be fully accessible in solution.

Neutralization of VSV-SARS-CoV-2-$S_{\Delta 21}$ and SARS-CoV-2 by human immune serum. As part of studies to evaluate immune convalescent plasma as a possible therapy for SARS-CoV-2 infected patients (Bloch et al., 2020), we obtained 42 serum samples from 20 individuals at different time points after the onset of COVID-19 symptoms (**Table 1**). These samples were pre-screened using a commercially available IgG ELISA. We tested each sample for neutralization of VSV-SARS-CoV-2-$S_{\Delta 21}$ and SARS-CoV-2 on Vero E6 cells. We observed that sera with ELISA negative or indeterminate results generally showed low inhibitory titers (EC_{50} <1/100), whereas ELISA positive sera generated a broad range of neutralizing antibody activity (EC_{50} > 1/200 to

>1/1,900) (**Fig 4A and C, Fig S3**). Remarkably, neutralization of VSV-SARS-CoV-2-$S_{\Delta 21}$ and SARS-CoV-2 was similar across the entire panel of samples (**Fig 4B and C, Fig S3**).

VSV-SARS-CoV-2-$S_{\Delta 21}$ and SARS-CoV-2 neutralization assays are highly correlative. We determined the extent to which the VSV-SARS-CoV-2-$S_{\Delta 21}$ and SARS-CoV-2 neutralization tests correlated with each other. We compared the GRNT and FRNT EC_{50} values obtained in assays with mAbs, polyclonal sera, and soluble ACE2 protein (**Fig 5**). For the samples with neutralizing activity, we observed a remarkably strong correlation between the two assays (r = 0.9285; $p < 0.001$). Moreover, all 11 of the samples that were deemed non-neutralizing in one assay had the same result in the second assay. Together, these results establish the utility of using VSV-SARS-CoV-2-$S_{\Delta 21}$ as a surrogate for authentic SARS-CoV-2 infection in entry inhibition and neutralization studies.

DISCUSSION

Emerging viral pathogens have caused numerous epidemics and several pandemics over the last century. The most recent example, SARS-CoV-2, has spread to nearly every country in the world in just a few months, causing millions of infections and hundreds of thousands of deaths (https://www.worldometers.info/coronavirus/). Rapid responses to viral outbreaks and generation of countermeasures require readily accessible tools to facilitate study and evaluate antiviral activity. Here, we generated a high-titer, replication-competent chimeric VSV expressing the SARS-CoV-2 S protein that performs similarly to a SARS-CoV-2 clinical isolate across multiple neutralization tests. As access to BSL3 facilities is limited, the finding that VSV-SARS-CoV-2-$S_{\Delta 21}$ is neutralized similarly by decoy receptors, mAbs, and polyclonal antibodies in comparison to authentic SARS-CoV-2 is important. This tool will enable academic, government, and industry investigators to rapidly perform assays that interrogate SARS-CoV-2 entry, neutralization, and inhibition at a BSL2 level, which should simplify and expedite the discovery of therapeutic interventions and analysis of functional humoral immune responses.

Upon recovery of VSV-SARS-CoV-2-S_{AA}, we selected for a mutant, which contained a 21-amino acid deletion in the cytoplasmic tail. As truncation of the cytoplasmic tail eliminates the modified KxHxx ER retention signal, we suggest that this mutation facilitates more efficient incorporation of the SARS-CoV-2 S protein into the VSV particles. Although truncation of the cytoplasmic tail of HIV envelope protein resulted in conformational alterations in the ectodomain of the protein (Chen et al., 2015), based on the extensive neutralization data presented here including correlation to neutralization of a clinical isolate of SARS CoV-2, a 21-amino acid truncation does not appear to substantively alter the structure of the S protein ectodomain. It remains to be determined whether fully wild-type S protein can incorporate efficiently into VSV. Indeed, similar mutations were generated in the SARS-CoV S protein cytoplasmic tail to boost incorporation into retroviruses and VSV pseudotypes (Fukushi et al., 2005; Giroglou et al., 2004; Moore et al., 2004).

The value of a chimeric virus depends on its capacity to present viral surface antigens in a similar way to its authentic counterpart (Garbutt et al., 2004). Indeed, the morphology of the bullet-shaped rhabdovirus and the spherical coronavirus and the density and geometry of S protein display could differentially impact antibody engagement and neutralization. Despite this concern, our extensive testing of VSV-SARS-CoV-2-$S_{\Delta 21}$ with antibodies and soluble ACE2-Fc proteins showed similar neutralization profiles compared to authentic, fully infectious SARS-CoV-2. Thus, VSV-SARS-CoV-2-$S_{\Delta 21}$, despite the structural differences of the virion, provides a useful tool for screening antibodies, entry-based antiviral agents, and vaccine responses against SARS-CoV-2. Indeed, convalescent plasma is under investigation as a potential COVID-19 therapeutic (Chen et al., 2020). Our studies suggest that in addition to testing for anti-S or anti-RBD antibodies (Shen et al., 2020), neutralization assays with VSV-SARS-CoV-2-$S_{\Delta 21}$ may be a convenient and rapid method to obtain functional information about immune plasma preparations to enable prioritization prior to passive transfer to COVID-19 patients.

Coronaviruses possess a roughly 30 kb RNA genome, which requires that they encode a proofreading enzyme (ExoN in nsp14) (Denison et al., 2011) to counteract the error rate of the viral RNA-dependent RNA polymerase. The lack of such proofreading enzymes in the genomes of rhabdoviruses suggests that selection of escape mutants to inhibitors of the coronavirus S protein will be faster in VSV-SARS-CoV-2, which further increases the utility of this chimeric virus. Our FRNT and GRNT assays can be used to establish evidence of prior SARS-CoV-2 infection or vaccination, as well as determine waning of functional responses over time, as the likelihood of cross-neutralizing responses with other cosmopolitan coronaviruses (*e.g.*, HCoV-229E and HCoV-OC43) is exceedingly low. Overall, VSV-SARS-CoV-2-$S_{\Delta 21}$ and our FRNT and GRNT assays, can facilitate the development and evaluation of antibody- or entry-based countermeasures against SARS-CoV-2 infection.

ACKNOWLEDGEMENTS

This study was supported by NIH contracts and grants (75N93019C00062, HHSN272201700060C and R01 AI127828, R37 AI059371 and U01 AI151810) and the Defense Advanced Research Project Agency (HR001117S0019) and gifts from Washington University in Saint Louis. J.B.C. is supported by a Helen Hay Whitney Foundation postdoctoral fellowship. We thank James Rini for providing RBD used to detect phage display mAbs. Some of the figures were created using BioRender.com.

AUTHOR CONTRIBUTIONS

J.B.C. performed SARS-CoV-2 neutralization experiments. P.W.R. generated and characterized VSV-SARS-CoV-2-$S_{\Delta 21}$ and performed neutralization experiments. R.E.C., Z.L., L.M.B., M.A.T., S.D., and Q.Z. provided experimental assistance. S.T., L.D., and D.W. prepared RNAseq libraries and assembled the VSV-SARS-CoV-2-$S_{\Delta 21}$ sequence. H.Z. and D.H.F. generated and provided purified proteins, D.C. and H.W.V. provided the recombinant mAbs, S.M. M.U. S.S., and G.A. provided other recombinant mAbs, E.S.T. and J.P.H. identified and provided the human immune serum. M.X.G.I. helped with automated microscope use and analysis. J.B.C, P.W.R., S.P.J.W., and M.S.D. wrote the initial draft, with the other authors providing editing comments.

COMPETING FINANCIAL INTERESTS

M.S.D. is a consultant for Inbios, Vir Biotechnology, NGM Biopharmaceuticals, and on the Scientific Advisory Board of Moderna. D.C. and H.W.V. are employees of Vir Biotechnology Inc. and may hold shares in Vir Biotechnology Inc. S.P.J.W. and P.W.R. have filed a disclosure with Washington University for the recombinant VSV.

FIGURE LEGENDS

Figure 1. Generation and characterization of an infectious VSV-SARS-CoV-2 chimera. (**A**) A schematic diagram depicting the genomic organization of the VSV recombinants, shown 3' to 5' are the leader region (Le), eGFP, nucleocapsid (N), phosphoprotein (P), matrix (M), glycoprotein (G) or SARS-CoV-2 S, large polymerase (L), and trailer region (Tr). (*Right panel*) Infection of Vero CCL81 cells with supernatant from cells transfected with the eGFP reporter VSV-SARS-CoV-2-S_{AA}. Images were acquired 44 hours post-infection (hpi) using a fluorescence microscope, and GFP and transmitted light images were merged using ImageJ. (*Bottom panel*) Alignment of the cytoplasmic tail of the VSV-SARS-CoV-2-S_{AA} and the sequence resulting from forward genetic selection of a mutant, which truncated the cytoplasmic tail by 21 amino acids. Mutations deviating from the wild-type spike are indicated in red, and an asterisk signifies a mutation to a stop codon. (**B**) Plaque assays were performed to compare the spread of VSV-SARS-CoV-2-S_{AA} rescue supernatant and VSV-SARS-CoV-2-$S_{\Delta 21}$ on Vero CCL81, Vero E6, Vero-furin, and MA104 cells. Plates were scanned on a biomolecular imager and expression of eGFP is shown 92 hpi (representative images are shown; n>3 except for S_{AA} on Vero E6, Vero-furin, and MA104 cells). (**C**) The indicated cell types were infected with VSV-SARS-CoV-2-$S_{\Delta 21}$ at an MOI of 0.5. Cells and supernatants were harvested at 24 hpi and titrated on MA104 cells (data are pooled from three or more independent experiments). (**D**) (*Top panel*) The indicated cells were infected with VSV-SARS-CoV-2-$S_{\Delta 21}$ at an MOI of 2. Images were acquired 7.5 hpi using a fluorescence microscope and GFP, and transmitted light images were processed and merged using ImageJ (data are representative of two independent experiments). (*Bottom panel*) Plaque assays were performed on the indicated cell types using VSV-SARS-CoV-2-$S_{\Delta 21}$. Images showing GFP expression were acquired 48 hpi using a biomolecular imager (data are representative of at least 3 independent experiments). (**E**) Western blotting was performed on concentrated VSV-SARS-CoV-2-$S_{\Delta 21}$ and wild-type VSV particles on an 8% non-reducing SDS-PAGE gel. S1 was detected using a cross-reactive anti-SARS-CoV mAb (CR3022) (data are representative of two

311 independent experiments). (**F**) BSRT7/5 cells were inoculated at an MOI of 10 with VSV-eGFP,
312 G-complemented VSV-SARS-CoV-2-$S_{\Delta 21}$, or mock infected (not shown), and metabolically
313 labeled with [^{35}S] methionine and cysteine for 20 h starting at 5 hpi in the presence of actinomycin
314 D. Viral supernatants were analyzed by SDS-PAGE. A representative phosphor-image is shown
315 from two independent experiments. An asterisk indicates a band that also was detected in the
316 mock lane (not shown). (**G**) Purified VSV-WT and VSV-SARS-CoV-2-$S_{\Delta 21}$ particles were
317 subjected to negative stain electron microscopy. Prefusion structures of each respective
318 glycoprotein are modeled above each EM image (PDB: 5I2S and 6VSB).

319 **Figure 2. Development of a SARS-CoV-2 focus-forming assay and a VSV-SARS-**
320 **CoV-2-$S_{\Delta 21}$ eGFP-reduction assay.** (**A**) Representative focus forming assay images of viral
321 stocks generated from each producer cell type (top) were developed on the indicated cell
322 substrates (indicated on the left side). Data are representative of two independent experiments.
323 Foci obtained in (**A**) were counted (**B**) and the size was determined (**C**) using an ImmunoSpot
324 plate reader (* $P < 0.05$, ** $P < 0.01$, *** $P < 0.001$ 1 by One-way ANOVA with Tukey's multiple
325 comparisons test). (**D**) Representative serial dilution series of VSV-SARS-CoV-2-$S_{\Delta 21}$ on Vero E6
326 cells. The total number of infected cells per well was quantified using an automated microscope.
327 Insets of enhanced magnification are shown in red. Data are representative of two independent
328 experiments.

329 **Figure 3. Neutralization of VSV-SARS-CoV-2-$S_{\Delta 21}$ and SARS-CoV-2 by human**
330 **monoclonal antibodies and hACE2 decoy receptors. A-B.** Cross-reactive mAbs isolated from
331 a SARS-CoV survivor were tested for neutralizing activity against SARS-CoV-2 (**A**) or VSV-
332 SARS-CoV-2-$S_{\Delta 21}$ (**B**) (n=2 and 3, respectively). **C-D**. SARS-CoV-2 RBD-specific antibodies
333 obtained from a phage library were tested for their capacity to neutralize SARS-CoV-2 (**C**) or VSV-
334 SARS-CoV-2-$S_{\Delta 21}$ (**D**) (n=2 and 2, respectively). **E-F**. hACE2-Fc or mACE2-Fc were tested for
335 their neutralization activity against SARS-CoV-2 (**E**) or VSV-SARS-CoV-2-$S_{\Delta 21}$ (**F**) (n=2 and 3,
336 respectively).

Figure 4. Human immune serum neutralization of SARS-CoV-2 and VSV-SARS-CoV-2-$S_{\Delta 21}$. Representative neutralization curves of serum from SARS-CoV-2-infected donors with low, medium, and high inhibitory activity against SARS-CoV-2 (**A**) or VSV-SARS-CoV-2-$S_{\Delta 21}$ (**B**) (n=2 and 2, respectively). (**C**) EC_{50} values of all human serum tested for neutralization of SARS-CoV-2 and VSV-SARS-CoV-2-$S_{\Delta 21}$. Differences in the geometric mean or median titers were less than 3-fold between FRNT and GRNT assays.

Figure 5. Correlation analysis of neutralization of SARS-CoV-2 and VSV-SARS-CoV-2-$S_{\Delta 21}$. EC_{50} values determined in **Fig 3A-D**, and **4A-B** were used to determine correlation between neutralization assays. Spearman's correlation *r* and *p* values are indicated.

SUPPLEMENTARY FIGURE LEGENDS

Figure S1. Rescue of a chimeric VSV expressing the SARS-CoV-2 S protein and forward genetic selection of a gain-of-function mutant. (**A**) BSRT7/5 cells were infected with vaccinia virus vTF7-3, transfected with plasmids allowing T7-driven expression of VSV N, P, L, and G, and an infectious molecular cDNA of VSV-SARS-CoV-2-S_{AA} to produce replication-competent VSV-SARS-CoV-2-S_{AA}. (**B**) Alignment of the membrane proximal region, transmembrane domain, and cytoplasmic tail of various recombinants that were generated. Successful rescue and indication of spread are noted. (**C**) VSV-SARS-CoV-2-S_{AA} was passaged iteratively on Vero CCL81 cells. Several clones were plaque-purified and amplified on Vero CCL81 cells. RNA from infected cells was extracted and deep sequenced to identify mutants.

Figure S2. Inhibition of VSV-SARS-CoV-2-$S_{\Delta 21}$ but not VSV with hACE2-Fc receptor decoy proteins. VSV-SARS-CoV-2-$S_{\Delta 21}$ and VSV were incubated with the indicated human or murine ACE2-Fc receptor decoy proteins, and virus-antibody mixtures were used to infect Vero E6 cells in a GRNT assay. Data are representative of three independent experiments.

Figure S3. Human immune serum neutralization of SARS-CoV-2 and VSV-SARS-CoV-2-$S_{\Delta 21}$. As described in **Fig 4**, human serum samples from PCR confirmed SARS-CoV-2-

363 infected patients were tested in FRNT (**A-G**) and GRNT (**H-N**) assays with SARS-CoV-2 and VSV-

364 SARS-CoV-2-$S_{\Delta 21}$.

365

METHODS

Plasmids. The S gene of SARS-CoV-2 isolate Wuhan-Hu-1 (GenBank MN908947.3) was synthesized in two fragments (Integrated DNA Technologies) and inserted into an infectious molecular clone of VSV (Whelan et al., 1995) as previously (Carette et al., 2011; Jae et al., 2014). Modifications to the cytoplasmic tail were assembled identically. Other plasmids were previously described: VSV N, P, L and G expression plasmids (Stanifer et al., 2011; Whelan et al., 1995), psPAX2 (Addgene), and pLX304-TMPRSS2 (Zang et al., 2020).

Cells. Cells were maintained in humidified incubators at 34 or 37°C and 5% CO_2 in the indicated media. BSRT7/5, Vero CCL81, Vero E6, Vero E6-TMPRSS2, A549, Caco-2, Caco-2 BBe1, Huh7, HepG2, Hela, BHK-21, HEK293, and HEK293T were maintained in DMEM (Corning or VWR) supplemented with glucose, L-glutamine, sodium pyruvate, and 10% fetal bovine serum (FBS). Vero-furin cells (Mukherjee et al., 2016) also were supplemented with 5 µg/ml of blasticidin. MA104 cells were maintained in Medium 199 (Gibco) containing 10% FBS. HT-29 cells were cultured in complete DMEM/F12 (Thermo-Fisher) supplemented with sodium pyruvate, non-essential amino acids, and HEPES. Vero E6-TMPRSS2 cells were generated using a lentivirus vector. Briefly, HEK293T producer cells were transfected with pLX304-TMPRSS2, pCAGGS-VSV-G, and psPAX2, and cell culture supernatants were collected at 48 hours and clarified by centrifugation at 1,000 x g for 5 min. The resulting lentivirus was used to infect Vero E6 cells for 24 h, and cells were selected with 40 µg/ml blasticidin for 7 days.

Recombinant VSV. Recovery of recombinant VSV was performed as described (Whelan et al., 1995). Briefly, BSRT7/5 cells were inoculated with vaccinia virus vTF7-3 and subsequently transfected with T7-expression plasmids encoding VSV N, P, L, and G, and an antigenomic copy of the viral genome. Cell culture supernatants were collected at 56-72 h, clarified by centrifugation (5 min at 1,000 x g), and filtered through a 0.22 µm filter. Virus was plaque-purified on Vero CCL81 cells in the presence of 25 µg/ml of cytosine arabinoside (TriLink BioTechnologies), and plaques in agarose plugs were amplified on Vero CCL81 cells. Viral stocks were amplified on MA104 cells

at an MOI of 0.01 in Medium 199 containing 2% FBS and 20 mM HEPES pH 7.7 (Millipore Sigma) at 34°C. Viral supernatants were harvested upon extensive cytopathic effect and clarified of cell debris by centrifugation at 1,000 x g for 5 min. Aliquots were maintained at -80°C.

Next generation sequencing. Total RNA was extracted from Vero CCL81 cells infected with VSV-SARS-CoV-2-$S_{\Delta 21}$ using Trizol (Invitrogen) according to the manufacturer's protocol. RNA was used to generate next generation sequencing libraries using TruSeq Stranded Total RNA library kit with Ribo Zero ribosomal subtraction (Illumina). The libraries were quantified using a bioanalyzer (Agilent) and pooled at an equal molar concentration and used to generate paired end 250 bp reads on an MiSeq (Illumina). Raw sequencing data was processed using fastp v0.20.0 to trim adapters and filter out reads with a quality score < 30. Alignment of each sample to VSV and SARS CoV-2 sequence was performed using bbmap v38.79. Mapped reads were extracted using samtools 1.9 and used for de novo assembly by SPAdes v3.13.0. Consensus sequences for each RNA sample were generated by aligning contigs to the reference plasmid sequence pVSV(1+)-eGFP-SARS-CoV-2-S with SnapGene v5.0.

Western blotting. Purified VSV were incubated in non-reducing denaturation buffer (55 mM Tris-HCl pH 6.8, 1.67 % (w/v) SDS, 7.5 % (w/v) glycerol) at 100°C for 5 min. Viral proteins were separated on a 8% acrylamide gel, transferred onto a nitrocellulose membrane, and incubated with human anti-SARS antibody CR3022 diluted in Tris-buffer saline containing 1% Tween-20 (TBS-T) and 5% milk, followed by incubation with HRP-conjugated goat anti-human antibody (Abcam) diluted in TBS-T containing 1% milk. HRP activity was visualized using the Pierce ECL Western blotting kit (Thermo Scientific) and imaged with a ChemiDocTM MP Imager (Bio-Rad).

Metabolic radiolabeling of virions. To generate high titer stocks of VSV-SARS-CoV-2, BSRT7/5 cells were transfected with pCAGGS-VSV-G in Opti-MEM (Gibco) using Lipofectamine 2000 (Invitrogen) and infected 7 h later with VSV-SARS-CoV-2-SΔ21 at an MOI of 0.1 in DMEM containing 2% FBS and 20 mM HEPES pH 7.7. Viral stocks were collected at 48 hpi, and used to

infect fresh cells (MOI of 10) for labeling of viral proteins. At 4 hpi, cells were starved in serum free, methionine/cysteine free DMEM (Corning), and exposed to 15 µCi/ml [^{35}S]-methionine and [^{35}S]-cysteine (Perkin Elmer) from 5-24 hours. Cell culture supernatants were collected, clarified by centrifugation (1,500 x g, 5 min), and analyzed by SDS-PAGE and detected by phosphoimage analysis (Li et al., 2006).

Transmission electron microscopy. Purified viruses were adhered to glow-discharged, carbon-coated copper grids. Samples were stained with 2% (w/v) phosphotungstic acid, pH 7.1, in H_2O and viewed on a JEOL 1200 EX transmission electron microscope (JEOL USA Inc.) equipped with an AMT 8-megapixel digital camera and AMT Image Capture Engine V602 software (Advanced Microscopy Techniques).

Monoclonal antibodies. Phage-displayed Fab libraries were panned against immobilized SARS-CoV-2 spike RBD in multiple rounds using established methods (Persson et al., 2013). Following four rounds of selection, phage ELISAs were used to screen 384 clones to identify those that bound specifically to RBD. The complementarity determining regions of Fab-phage clones were decoded by sequencing the variable regions and cloning them into mammalian expression vectors for expression and purification of human IgG1 proteins, as described (Tao et al., 2019). A subset of the panel of mAbs was tested for neutralization as a part of this study.

Another set of mAbs (S304, S306, S309, S310 and S315) were isolated from EBV-immortalized memory B cells from a SARS-CoV survivor (Traggiai et al., 2004) and are cross-reactive to SARS-CoV-2 (Pinto et al, in press). Recombinant antibodies were expressed in ExpiCHO cells transiently co-transfected with plasmids expressing the heavy and light chain as previously described (Stettler et al., 2016).

Human sera. Human samples were collected from PCR-confirmed COVID-19 patients. Serum samples were obtained by routine phlebotomy at different days post symptom onset (range: day 5 - 20). Samples were prescreened by the Euroimmun anti-SARS-CoV-2 IgG ELISA (Lubeck, Germany), a qualitative assay with the Food and Drug Administration Emergency Use

Authorization that detects antibodies to the SARS-CoV-2 S protein. This study was approved by the Mayo Clinic Institutional Review Board.

Protein expression and purification. DNA fragments encoding human ACE2 (hACE2 residues 1-615) and mouse ACE2 (mACE2, residues 1-615) were synthesized and cloned into pFM1.2 with a C-terminal HRV-3C protease cleavage site (LEVLFQGP) and a human IgG1 Fc region as previously described (Raj et al., 2013). We transiently transfected plasmids into Expi293F cells and harvested cell supernatants 4 days post transfection. Secreted hACE2-Fc and mACE2-Fc proteins were purified by protein A chromatography (Goldbio).

GFP-reduction neutralization test. Patient samples were heat-inactivated at 56°C for 30 min. Indicated dilutions of samples were incubated with 10^2 PFU of VSV-SARS-CoV-2-$S_{\Delta 21}$ for 1 h at 37°C. Antibody-virus complexes were added to Vero E6 cells in 96-well plates and incubated at 37°C for 7.5 h. Cells subsequently were fixed in 2% formaldehyde containing 10 µg/mL Hoechst 33342 nuclear stain (Invitrogen) for 45 min at room temperature, when fixative was replaced with PBS. Images were acquired with the InCell 2000 Analyzer (GE Healthcare) automated microscope in both the DAPI and FITC channels to visualize nuclei and infected cells (*i.e.*, eGFP-positive cells), respectively (4X objective, 4 fields per well, covering the entire well). Images were analyzed using the Multi Target Analysis Module of the InCell Analyzer 1000 Workstation Software (GE Healthcare). GFP-positive cells were identified in the FITC channel using the top-hat segmentation method and subsequently counted within the InCell Workstation software. The sensitivity and accuracy of GFP-positive cell number determinations were validated using a serial dilution of virus. A background number of GFP+ cells was subtracted from each well using an average value determined from at least 4 uninfected wells. Data were processed using Prism software (GraphPad Prism 8.0). ACE2 neutralization assays using VSV-SARS-CoV-2-$S_{\Delta 21}$ were conducted similarly but using an MOI of 1.

Focus reduction neutralization test. SARS-CoV-2 strain 2019 n-CoV/USA_WA1/2020 was obtained from the Centers for Disease Control and Prevention (gift of Natalie Thornburg). Virus was passaged in the indicated producer cells. Indicated dilutions of mAbs, sera, or protein were incubated with 10^2 FFU of SARS-CoV-2 for 1 h at 37°C. Antibody-virus complexes were added to indicated cell monolayers in 96-well plates and incubated at 37°C for 1 h. Subsequently, cells were overlaid with 1% (w/v) methylcellulose in MEM supplemented with 2% FBS. Plates were harvested 30 h later by removing overlays and fixed with 4% paraformaldehyde in PBS for 20 min at room temperature. Plates were washed and sequentially incubated with 1 µg/mL of CR3022 anti-S antibody (ter Meulen et al., 2006; Yuan et al., 2020) and HRP-conjugated goat anti-human IgG in PBS supplemented with 0.1% saponin and 0.1% BSA. SARS-CoV-2-infected cell foci were visualized using TrueBlue peroxidase substrate (KPL) and quantitated on an ImmunoSpot microanalyzer (Cellular Technologies). Data were processed using Prism software (GraphPad Prism 8.0).

Statistical analyses. All statistical tests were performed using GraphPad Prism 8.0 software as described in the indicated figure legends.

REFERENCES

Bai, Y., Yao, L., Wei, T., Tian, F., Jin, D.Y., Chen, L., and Wang, M. (2020). Presumed Asymptomatic Carrier Transmission of COVID-19. JAMA.

Bloch, E.M., Shoham, S., Casadevall, A., Sachais, B.S., Shaz, B., Winters, J.L., van Buskirk, C., Grossman, B.J., Joyner, M., Henderson, J.P., *et al.* (2020). Deployment of convalescent plasma for the prevention and treatment of COVID-19. J Clin Invest.

Carette, J.E., Raaben, M., Wong, A.C., Herbert, A.S., Obernosterer, G., Mulherkar, N., Kuehne, A.I., Kranzusch, P.J., Griffin, A.M., Ruthel, G., *et al.* (2011). Ebola virus entry requires the cholesterol transporter Niemann-Pick C1. Nature *477*, 340-343.

Chen, J., Kovacs, J.M., Peng, H., Rits-Volloch, S., Lu, J., Park, D., Zablowsky, E., Seaman, M.S., and Chen, B. (2015). HIV-1 ENVELOPE. Effect of the cytoplasmic domain on antigenic characteristics of HIV-1 envelope glycoprotein. Science *349*, 191-195.

Chen, L., Xiong, J., Bao, L., and Shi, Y. (2020). Convalescent plasma as a potential therapy for COVID-19. Lancet Infect Dis *20*, 398-400.

Denison, M.R., Graham, R.L., Donaldson, E.F., Eckerle, L.D., and Baric, R.S. (2011). Coronaviruses: an RNA proofreading machine regulates replication fidelity and diversity. RNA biology *8*, 270-279.

Fukushi, S., Mizutani, T., Saijo, M., Kurane, I., Taguchi, F., Tashiro, M., and Morikawa, S. (2006). Evaluation of a novel vesicular stomatitis virus pseudotype-based assay for detection of neutralizing antibody responses to SARS-CoV. J Med Virol *78*, 1509-1512.

Fukushi, S., Mizutani, T., Saijo, M., Matsuyama, S., Miyajima, N., Taguchi, F., Itamura, S., Kurane, I., and Morikawa, S. (2005). Vesicular stomatitis virus pseudotyped with severe acute respiratory syndrome coronavirus spike protein. J Gen Virol *86*, 2269-2274.

Garbutt, M., Liebscher, R., Wahl-Jensen, V., Jones, S., Moller, P., Wagner, R., Volchkov, V., Klenk, H.D., Feldmann, H., and Stroher, U. (2004). Properties of replication-competent vesicular stomatitis virus vectors expressing glycoproteins of filoviruses and arenaviruses. J Virol *78*, 5458-5465.

Giroglou, T., Cinatl, J., Jr., Rabenau, H., Drosten, C., Schwalbe, H., Doerr, H.W., and von Laer, D. (2004). Retroviral vectors pseudotyped with severe acute respiratory syndrome coronavirus S protein. J Virol *78*, 9007-9015.

Guan, W.J., Ni, Z.Y., Hu, Y., Liang, W.H., Ou, C.Q., He, J.X., Liu, L., Shan, H., Lei, C.L., Hui, D.S.C., *et al.* (2020). Clinical Characteristics of Coronavirus Disease 2019 in China. N Engl J Med *382*, 1708-1720.

Hoffmann, M., Kleine-Weber, H., Schroeder, S., Kruger, N., Herrler, T., Erichsen, S., Schiergens, T.S., Herrler, G., Wu, N.H., Nitsche, A., *et al.* (2020). SARS-CoV-2 Cell Entry Depends on ACE2 and TMPRSS2 and Is Blocked by a Clinically Proven Protease Inhibitor. Cell *181*, 271-280.

Jae, L.T., Raaben, M., Herbert, A.S., Kuehne, A.I., Wirchnianski, A.S., Soh, T.K., Stubbs, S.H., Janssen, H., Damme, M., Saftig, P.*, et al.* (2014). Virus entry. Lassa virus entry requires a trigger-induced receptor switch. Science *344*, 1506-1510.

Kobinger, G.P., Limberis, M.P., Somanathan, S., Schumer, G., Bell, P., and Wilson, J.M. (2007). Human immunodeficiency viral vector pseudotyped with the spike envelope of severe acute respiratory syndrome coronavirus transduces human airway epithelial cells and dendritic cells. Hum Gene Ther *18*, 413-422.

Kruse, R.L. (2020). Therapeutic strategies in an outbreak scenario to treat the novel coronavirus originating in Wuhan, China. F1000Research *9*, 72.

Lei, C., Qian, K., Li, T., Zhang, S., Fu, W., Ding, M., and Hu, S. (2020). Neutralization of SARS-CoV-2 spike pseudotyped virus by recombinant ACE2-Ig. Nat Commun *11*, 2070.

Letko, M., Marzi, A., and Munster, V. (2020). Functional assessment of cell entry and receptor usage for SARS-CoV-2 and other lineage B betacoronaviruses. Nature microbiology *5*, 562-569.

Li, F., Li, W., Farzan, M., and Harrison, S.C. (2005). Structure of SARS coronavirus spike receptor-binding domain complexed with receptor. Science *309*, 1864-1868.

Li, J., Wang, J.T., and Whelan, S.P. (2006). A unique strategy for mRNA cap methylation used by vesicular stomatitis virus. Proc Natl Acad Sci U S A *103*, 8493-8498.

Li, W., Moore, M.J., Vasilieva, N., Sui, J., Wong, S.K., Berne, M.A., Somasundaran, M., Sullivan, J.L., Luzuriaga, K., Greenough, T.C.*, et al.* (2003). Angiotensin-converting enzyme 2 is a functional receptor for the SARS coronavirus. Nature *426*, 450-454.

Lontok, E., Corse, E., and Machamer, C.E. (2004). Intracellular targeting signals contribute to localization of coronavirus spike proteins near the virus assembly site. J Virol *78*, 5913-5922.

McBride, C.E., Li, J., and Machamer, C.E. (2007). The cytoplasmic tail of the severe acute respiratory syndrome coronavirus spike protein contains a novel endoplasmic reticulum retrieval signal that binds COPI and promotes interaction with membrane protein. J Virol *81*, 2418-2428.

Moore, M.J., Dorfman, T., Li, W., Wong, S.K., Li, Y., Kuhn, J.H., Coderre, J., Vasilieva, N., Han, Z., Greenough, T.C.*, et al.* (2004). Retroviruses pseudotyped with the severe acute respiratory syndrome coronavirus spike protein efficiently infect cells expressing angiotensin-converting enzyme 2. J Virol *78*, 10628-10635.

Mukherjee, S., Sirohi, D., Dowd, K.A., Chen, Z., Diamond, M.S., Kuhn, R.J., and Pierson, T.C. (2016). Enhancing dengue virus maturation using a stable furin over-expressing cell line. Virology *497*, 33-40.

Ou, X., Liu, Y., Lei, X., Li, P., Mi, D., Ren, L., Guo, L., Guo, R., Chen, T., Hu, J.*, et al.* (2020). Characterization of spike glycoprotein of SARS-CoV-2 on virus entry and its immune cross-reactivity with SARS-CoV. Nat Commun *11*, 1620.

Persson, H., Ye, W., Wernimont, A., Adams, J.J., Koide, A., Koide, S., Lam, R., and Sidhu, S.S. (2013). CDR-H3 diversity is not required for antigen recognition by synthetic antibodies. J Mol Biol *425*, 803-811.

583 Pinto, D. Young-Jun Park, Martina Beltramello, Alexandra C. Walls, M. Alejandra Tortorici, Siro
584 Bianchi, Stefano Jaconi, Katja Culap, Fabrizia Zatta, Anna De Marco, Alessia Peter, Barbara
585 Guarino, Roberto Spreafico, Elisabetta Cameroni, James Brett Case, Rita E. Chen, Colin
586 Havenar-Daughton, Gyorgy Snell, Amalio Telenti, Herbert W. Virgin, Antonio Lanzavecchia,
587 Michael S. Diamond, Katja Fink, David Veesler and Davide Corti (2020). Cross-neutralization of
588 SARS-CoV and SARS-CoV-2 by a human monoclonal 2 antibody. Nature (in press)
589
590 Raj, V.S., Mou, H., Smits, S.L., Dekkers, D.H., Muller, M.A., Dijkman, R., Muth, D., Demmers,
591 J.A., Zaki, A., Fouchier, R.A.*, et al.* (2013). Dipeptidyl peptidase 4 is a functional receptor for the
592 emerging human coronavirus-EMC. Nature *495*, 251-254.
593
594 Ruch, T.R., and Machamer, C.E. (2012). The coronavirus E protein: assembly and beyond.
595 Viruses *4*, 363-382.
596
597 Shen, C., Wang, Z., Zhao, F., Yang, Y., Li, J., Yuan, J., Wang, F., Li, D., Yang, M., Xing, L.*, et al.*
598 (2020). Treatment of 5 Critically Ill Patients With COVID-19 With Convalescent Plasma. JAMA.
599
600 Stanifer, M.L., Cureton, D.K., and Whelan, S.P. (2011). A recombinant vesicular stomatitis virus
601 bearing a lethal mutation in the glycoprotein gene uncovers a second site suppressor that restores
602 fusion. J Virol *85*, 8105-8115.
603
604 Stettler, K., Beltramello, M., Espinosa, D.A., Graham, V., Cassotta, A., Bianchi, S., Vanzetta, F.,
605 Minola, A., Jaconi, S., Mele, F.*, et al.* (2016). Specificity, cross-reactivity, and function of
606 antibodies elicited by Zika virus infection. Science *353*, 823-826.
607
608 Tao, Y., Mis, M., Blazer, L., Ustav, M.J., Steinhart, Z., Chidiac, R., Kubarakos, E., O'Brien, S.,
609 Wang, X., Jarvik, N.*, et al.* (2019). Tailored tetravalent antibodies potently and specifically activate
610 Wnt/Frizzled pathways in cells, organoids and mice. Elife *8*.
611
612 ter Meulen, J., van den Brink, E.N., Poon, L.L., Marissen, W.E., Leung, C.S., Cox, F., Cheung,
613 C.Y., Bakker, A.Q., Bogaards, J.A., van Deventer, E.*, et al.* (2006). Human monoclonal antibody
614 combination against SARS coronavirus: synergy and coverage of escape mutants. PLoS Med *3*,
615 e237.
616
617 Tortorici, M.A., and Veesler, D. (2019). Structural insights into coronavirus entry. Adv Virus Res
618 *105*, 93-116.
619
620 Traggiai, E., Becker, S., Subbarao, K., Kolesnikova, L., Uematsu, Y., Gismondo, M.R., Murphy,
621 B.R., Rappuoli, R., and Lanzavecchia, A. (2004). An efficient method to make human monoclonal
622 antibodies from memory B cells: potent neutralization of SARS coronavirus. Nat Med *10*, 871-
623 875.
624
625 Walls, A.C., Park, Y.J., Tortorici, M.A., Wall, A., McGuire, A.T., and Veesler, D. (2020). Structure,
626 Function, and Antigenicity of the SARS-CoV-2 Spike Glycoprotein. Cell.
627
628 Watanabe, Y., Allen, J.D., Wrapp, D., McLellan, J.S., and Crispin, M. (2020). Site-specific glycan
629 analysis of the SARS-CoV-2 spike. Science.
630
631 Whelan, S.P., Ball, L.A., Barr, J.N., and Wertz, G.T. (1995). Efficient recovery of infectious
632 vesicular stomatitis virus entirely from cDNA clones. Proc Natl Acad Sci U S A *92*, 8388-8392.

633 Wrapp, D., Wang, N., Corbett, K.S., Goldsmith, J.A., Hsieh, C.L., Abiona, O., Graham, B.S., and
634 McLellan, J.S. (2020). Cryo-EM structure of the 2019-nCoV spike in the prefusion conformation.
635 Science.
636
637 Yuan, M., Wu, N.C., Zhu, X., Lee, C.D., So, R.T.Y., Lv, H., Mok, C.K.P., and Wilson, I.A. (2020).
638 A highly conserved cryptic epitope in the receptor-binding domains of SARS-CoV-2 and SARS-
639 CoV. Science.
640
641 Zang, R., Gomez Castro, M., McCune, B.T., Zeng, Q., Rothlauf, P.W., Sonnek, N.M., Liu, Z.,
642 Brulois, K.F., Wang, X., Greenberg, H.B.*, et al.* (2020). TMPRSS2 and TMPRSS4 promote SARS-
643 CoV-2 infection of human small intestinal enterocytes. Science Immunology, In press.
644
645 Zhang, T., Wu, Q., and Zhang, Z. (2020). Probable Pangolin Origin of SARS-CoV-2 Associated
646 with the COVID-19 Outbreak. Curr Biol.
647
648 Zhou, P., Yang, X.L., Wang, X.G., Hu, B., Zhang, L., Zhang, W., Si, H.R., Zhu, Y., Li, B., Huang,
649 C.L.*, et al.* (2020). A pneumonia outbreak associated with a new coronavirus of probable bat
650 origin. Nature *579*, 270-273.
651

Table 1. Human serum ELISA IgG.

Serum	Days post symptom onset	Euroimmun IgG		Epitope IgG	
		Index	Reactive	Index	Reactive
1	14	1.3	+	2.6	+
2	12	6.0	+	3.5	+
3	17	10.2	+	3.9	+
4	16	14.9	+	4.5	+
5	5	0.2	-	1.2	+
6	19	8.6	+	4.4	+
7	17	7.1	+	4.1	+
8	10	5.1	+	2.0	+
9	14	6.8	+	3.1	+
10	6	0.2	-	1.1	+
11	-	5.6	+	0.9	+/-
12	-	<0.8	-	1.3	+
13	9	0.7	-	1.1	+
14	20	3.6	+	2.9	+
15	13	0.4	-	2.0	+
16	13	0.5	-	0.9	-
17	11	0.3	-	0.8	-
18	10	0.2	-	0.7	-
19	14	0.9	+/-	1.2	+
20	10	0.4	-	1.5	+
21	11	0.5	-	2.0	+
22	10	0.3	-	0.6	-
23	17	7.6	+	4.2	+
24	14	3.5	+	3.3	+
25	13	1.5	+	2.9	+
26	17	14.2	+	4.4	+
27	13	0.5	-	1.9	+
28	14	9.2	+	4.6	+
29	13	3.9	+	2.8	+
30	16	3.4	+	4.6	+
31	15	10.7	+	3.6	+
32	6	0.5	-	1.1	+
33	11	0.4	-	1.8	+
34	12	0.6	-	2.5	+
35	14	3.7	+	4.1	+
36	20	11.6	+	4.2	+
37	7	0.7	-	1.2	+
38	8	1.7	+	1.9	+
39	7	0.3	-	0.7	-
40	9	3.4	+	2.2	+
41	18	10.3	+	4.1	+
42	17	10.3	+	4.6	+

Legend to Table 1: Serum samples from 20 individuals were collected at different time points post onset of COVID-19 symptoms, were screened using two ELISA assays (Euroimmun or Epitope). The serum numbers correspond to those of Figures 4 and S3. IgG index values were calculated by dividing the O.D. of the serum sample by a reference O.D. control, and ratios were interpreted using the following criteria as recommended by the manufacturer: Negative (-) <0.8, Indeterminate (+/-) 0.8-1.1, Positive (+) ≥1.1.

Fig 1

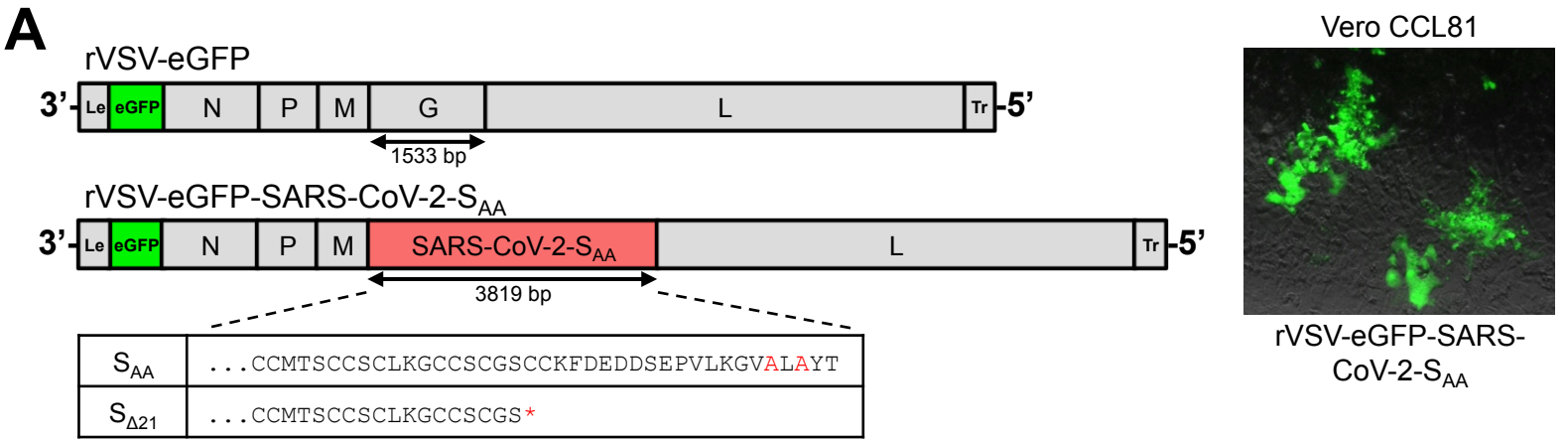
A
rVSV-eGFP
3'
Le
eGFP
N
P
M
G
L
Tr
5'
1533 bp
rVSV-eGFP-SARS-CoV-2-S$_{AA}$
SARS-CoV-2-S$_{AA}$
3819 bp
S$_{AA}$
...CCMTSCCSCLKGCCSCGSCCKFDEDDSEPVLKGVALAYT
S$_{\Delta 21}$
...CCMTSCCSCLKGCCSCGS*
Vero CCL81
rVSV-eGFP-SARS-CoV-2-S$_{AA}$

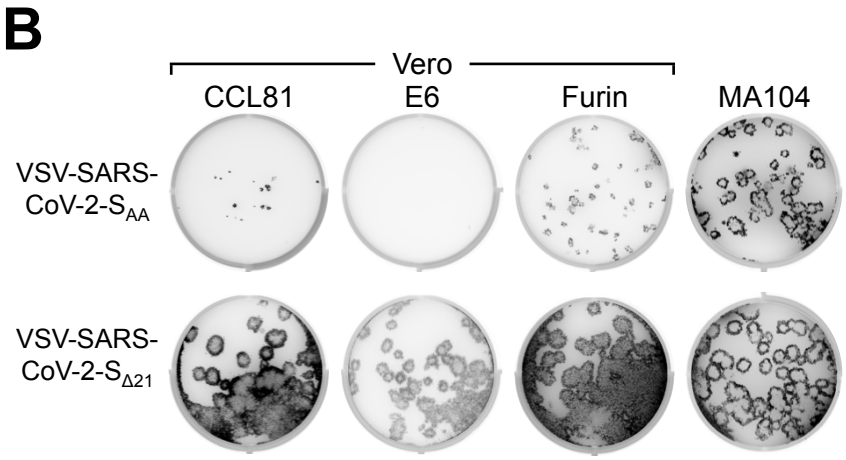
B
Vero
CCL81
E6
Furin
MA104
VSV-SARS-CoV-2-S$_{AA}$
VSV-SARS-CoV-2-S$_{\Delta 21}$

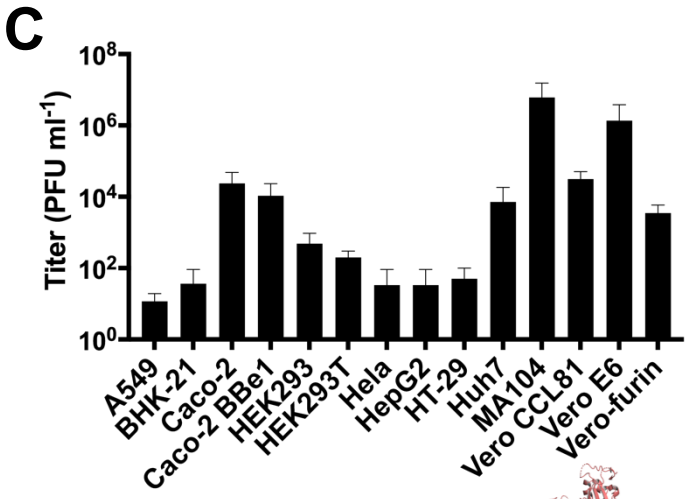
C
Titer (PFU ml^{-1})
10^8
10^6
10^4
10^2
10^0
A549
BHK-21
Caco-2
Caco-2 BBe1
HEK293
HEK293T
Hela
HepG2
HT-29
Huh7
MA104
Vero CCL81
Vero E6
Vero-furin

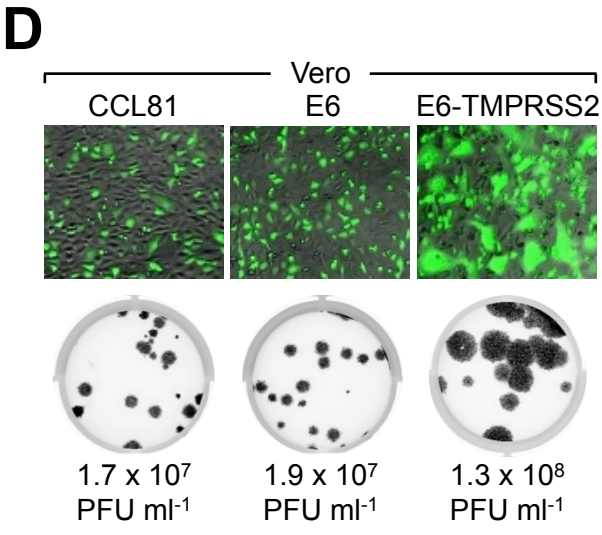
D
Vero
CCL81
E6
E6-TMPRSS2
1.7 x 10^7 PFU ml^{-1}
1.9 x 10^7 PFU ml^{-1}
1.3 x 10^8 PFU ml^{-1}

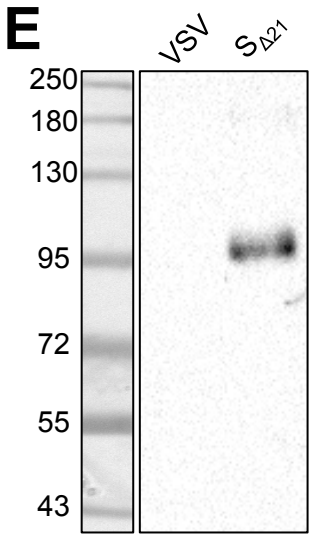
E
VSV
S$_{\Delta 21}$
250
180
130
95
72
55
43

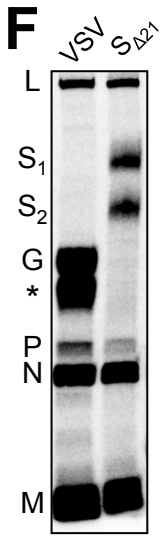
F
VSV
S$_{\Delta 21}$
L
S$_1$
S$_2$
G
*
P
N
M

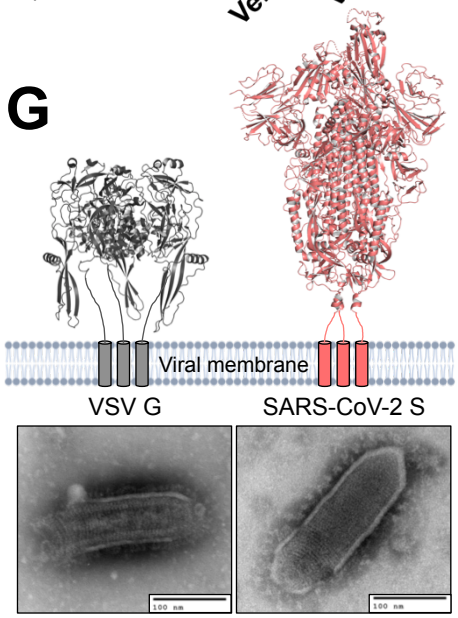
G
Viral membrane
VSV G
SARS-CoV-2 S

Fig 2

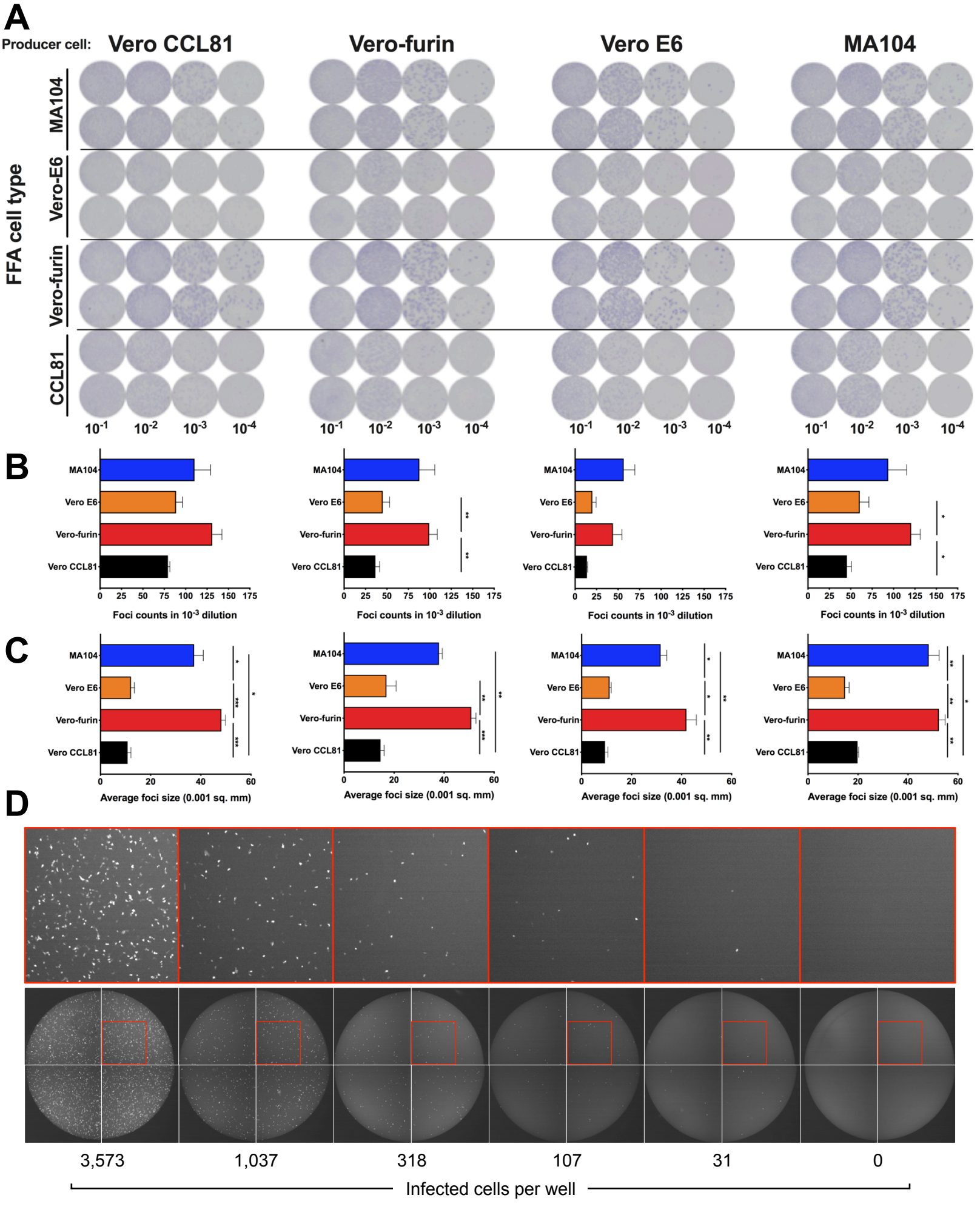
A
Producer cell:
Vero CCL81
Vero-furin
Vero E6
MA104
FFA cell type
MA104
Vero-E6
Vero-furin
CCL81
10-1 10-2 10-3 10-4
B
MA104
Vero E6
Vero-furin
Vero CCL81
0 25 50 75 100 125 150 175
Foci counts in 10-3 dilution
C
0 20 40 60
Average foci size (0.001 sq. mm)
D
3,573
1,037
318
107
31
0
Infected cells per well

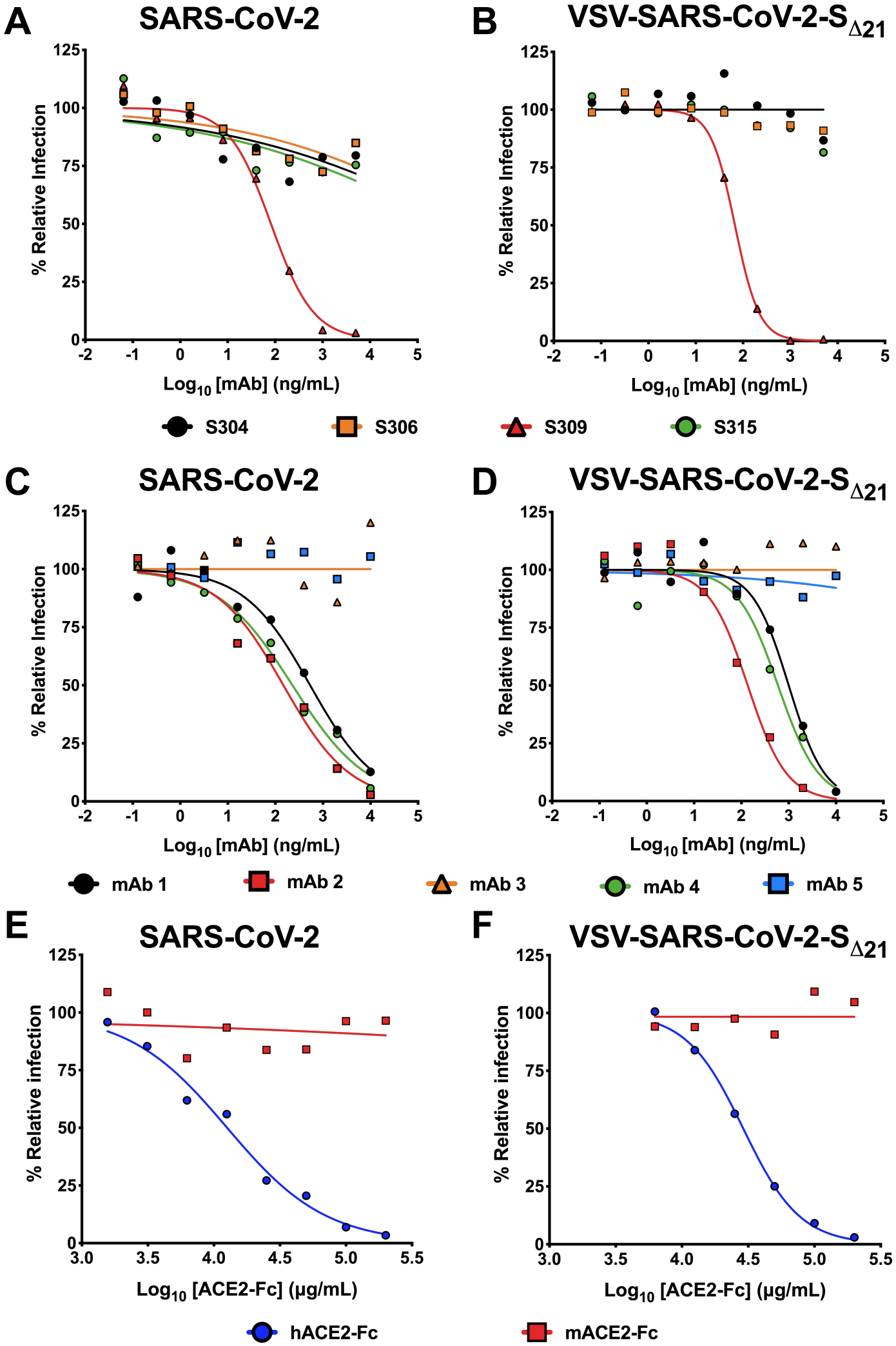
A
SARS-CoV-2
B
VSV-SARS-CoV-2-S$_{\Delta 21}$
% Relative Infection
Log$_{10}$ [mAb] (ng/mL)
S304
S306
S309
S315
C
SARS-CoV-2
D
VSV-SARS-CoV-2-S$_{\Delta 21}$
mAb 1
mAb 2
mAb 3
mAb 4
mAb 5
E
SARS-CoV-2
F
VSV-SARS-CoV-2-S$_{\Delta 21}$
% Relative infection
Log$_{10}$ [ACE2-Fc] (µg/mL)
hACE2-Fc
mACE2-Fc

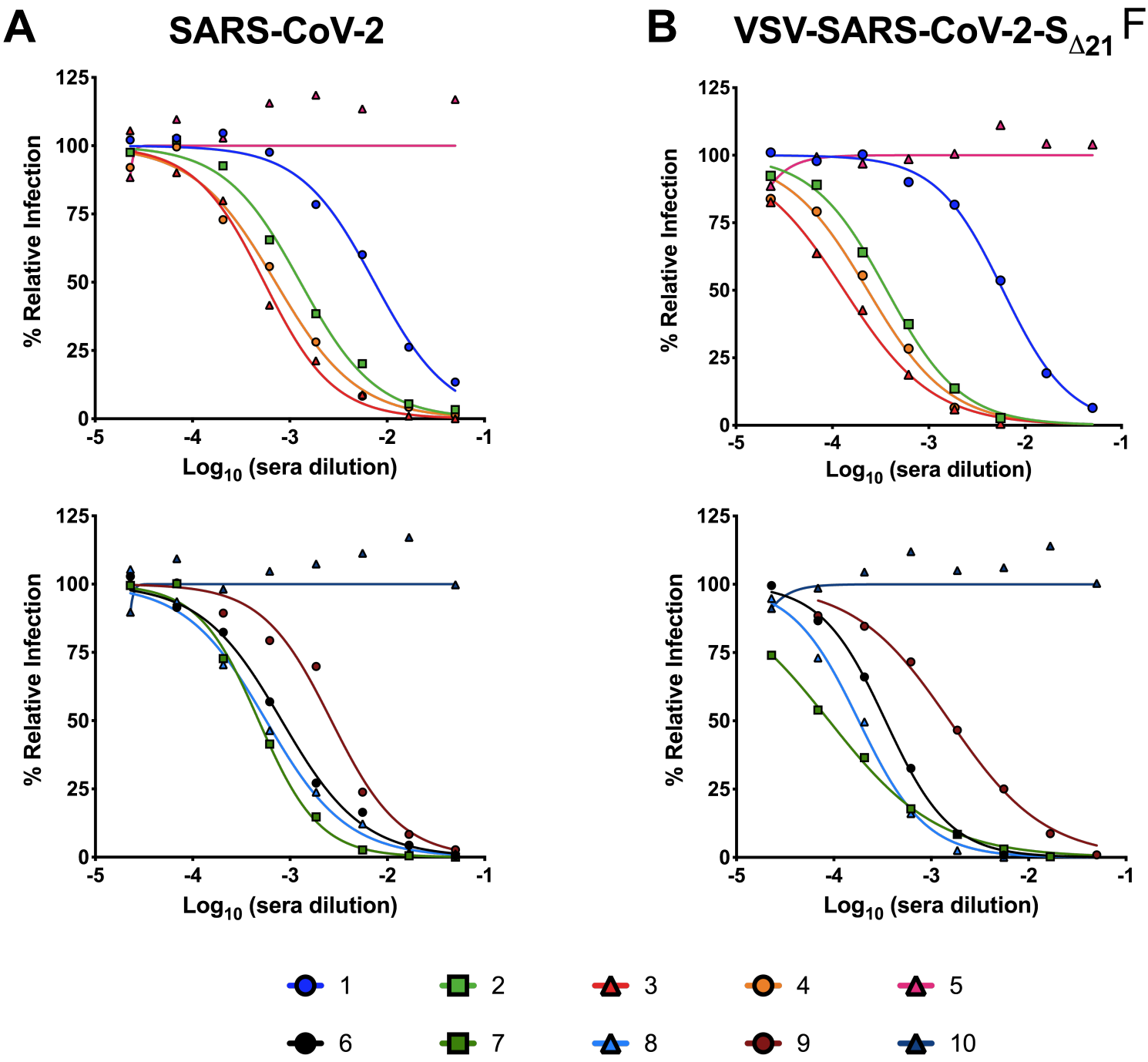
A
SARS-CoV-2
B
VSV-SARS-CoV-2-S$_{\Delta 21}$
% Relative Infection
Log$_{10}$ (sera dilution)
1
2
3
4
5
6
7
8
9
10

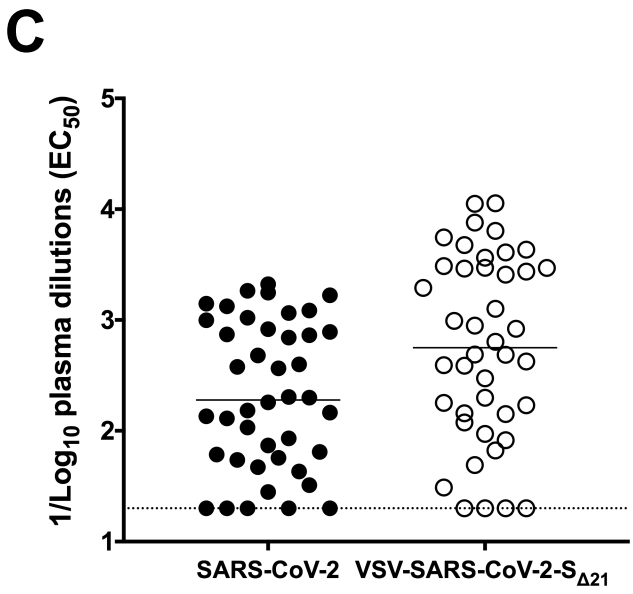
C
1/Log$_{10}$ plasma dilutions (EC$_{50}$)
SARS-CoV-2
VSV-SARS-CoV-2-S$_{\Delta 21}$

Fig 5

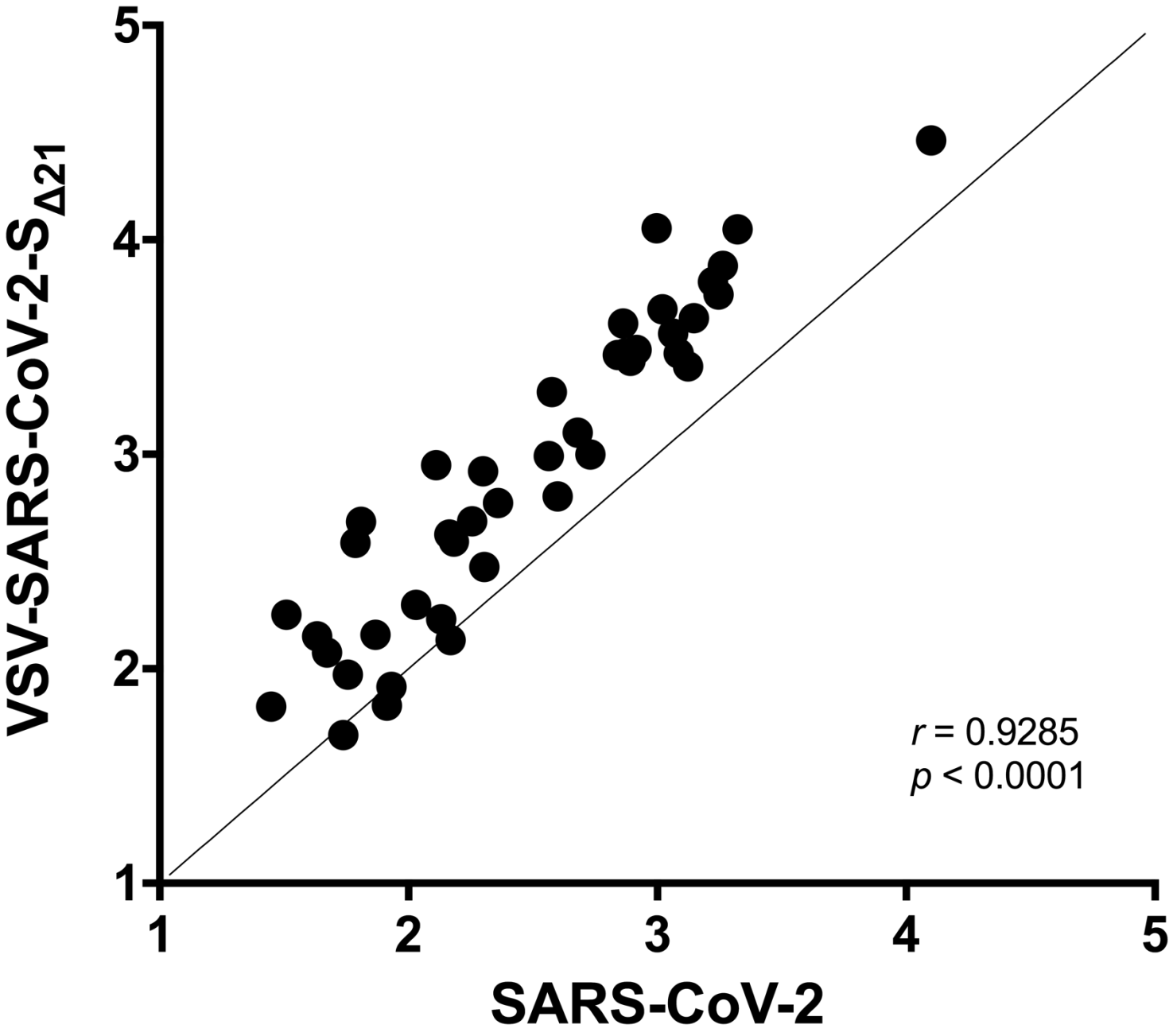

Fig S1

A

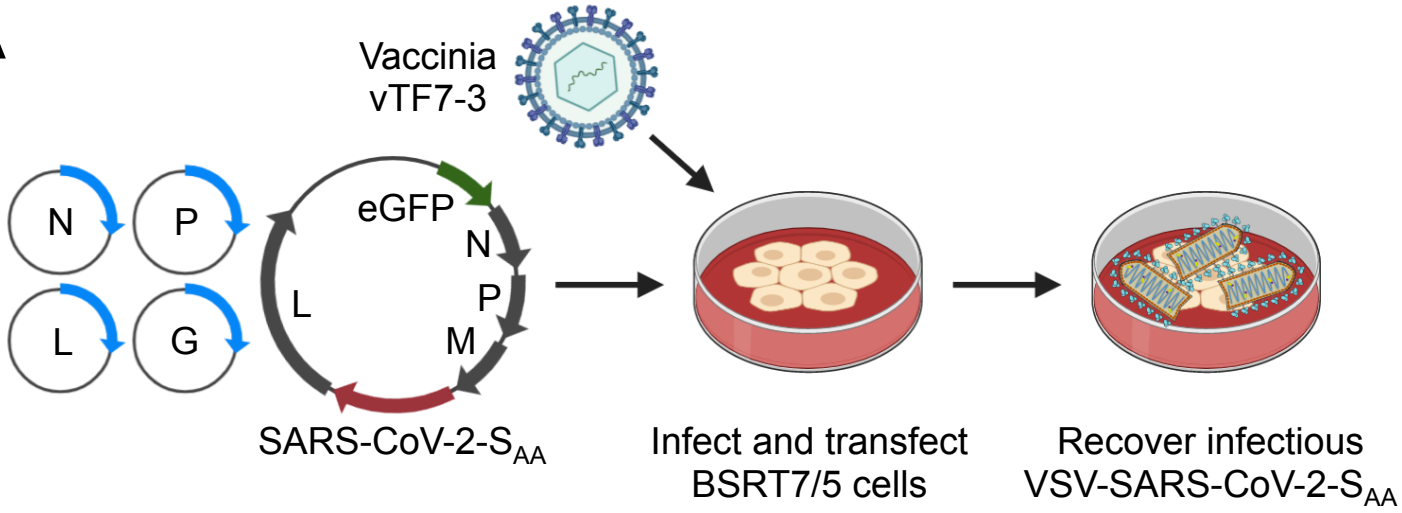

B

Tail Mutant	Amino acid sequence (membrane proximal region, transmembrane domain, cytoplasmic tail)	Rescue	Spread
S_{AA}	LNESLIDLQELGKYEQYIKWPWYIWLGFIAGLIAIVMVTIMLCCMTSCCSCLKGCCSCGSCCKFDEDDSEPVLKGVALAYT	+	+
MERS S_{AA}	LNESLIDLQELGKYEQYIKWPWYIWLGFIAGLIAIVMVTIMLKLKCNRCCDRYEEYDLEPHAVAVH	+	-
VSV G #1	LNESLIDLQELGKYEQYIKWPWYIWLGFIAGLIAIVMVTIMLCCMTSCCSCLRVGIYLCIKLKHTKKRQIYTDIEMNRLGK	+	-
VSV G #2	LNESLIDLQELGKYEQYIKWPWYIWLGFIAGLIAIVMVTIMLRVGIYLCIKLKHTKKRQIYTDIEMNRLGK	+	-
VSV G TM/tail	LNESLIDLQELGKYEQYIKWSSIASFCFIIGLIIGLFLVLRVGIYLCIKLKHTKKRQIYTDIEMNRLGK	+	-
VSV G Ecto/TM/tail	LNEGWFSSWKSSIASFCFIIGLIIGLFLVLRVGIYLCIKLKHTKKRQIYTDIEMNRLGK	+	-

C

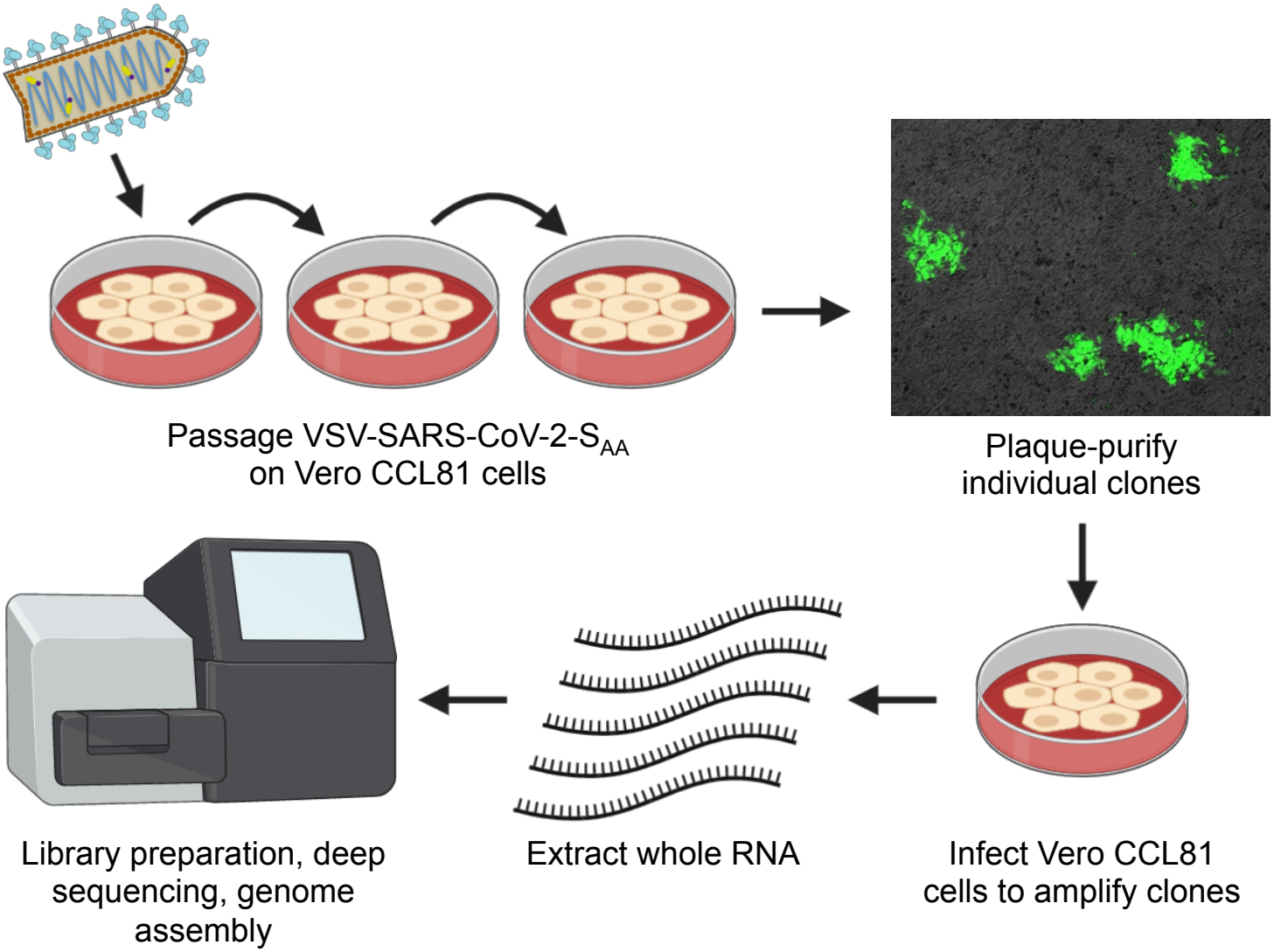

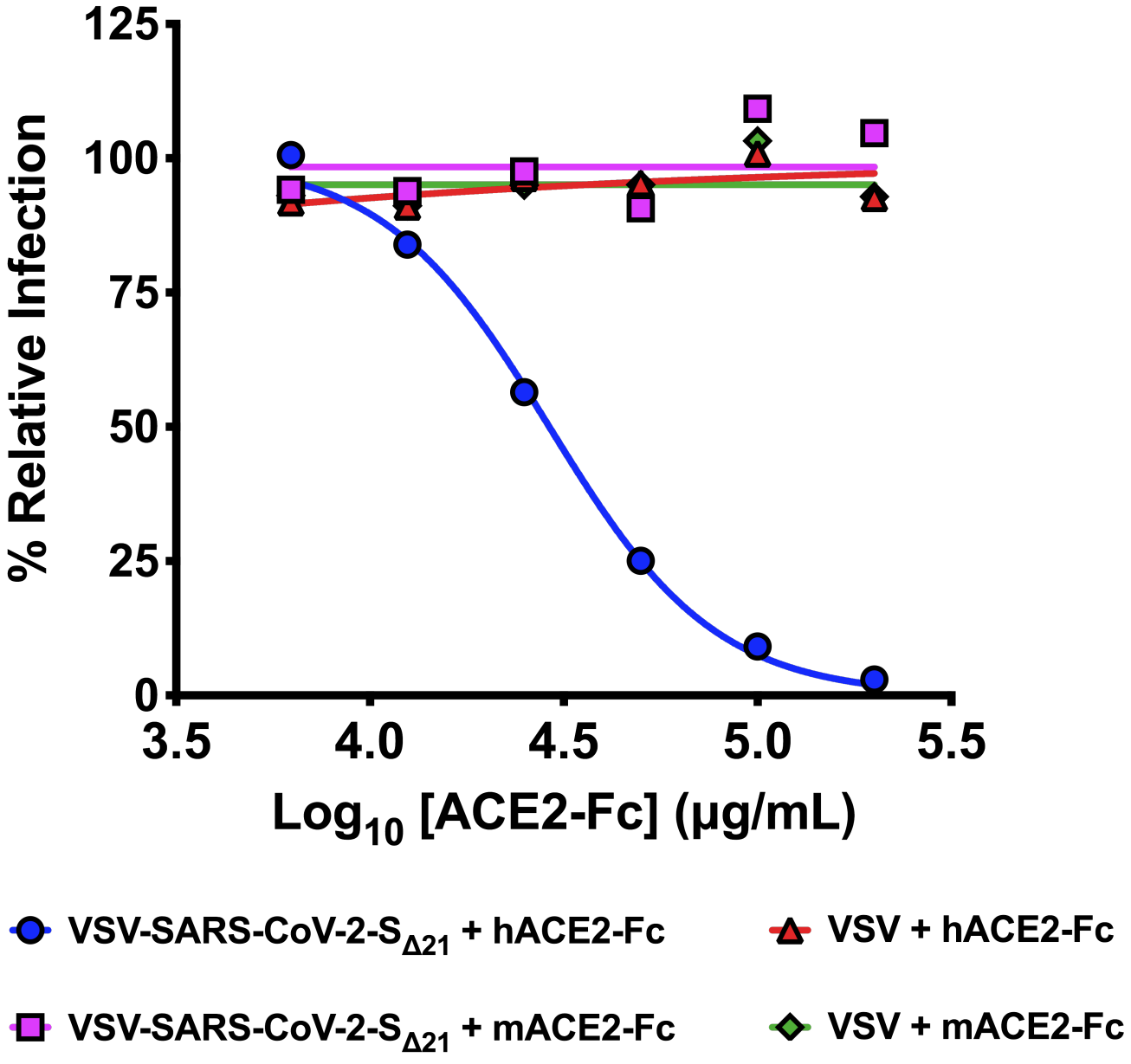
125
100
75
50
25
0
% Relative Infection
3.5
4.0
4.5
5.0
5.5
Log10 [ACE2-Fc] (µg/mL)
VSV-SARS-CoV-2-SΔ21 + hACE2-Fc
VSV + hACE2-Fc
VSV-SARS-CoV-2-SΔ21 + mACE2-Fc
VSV + mACE2-Fc

Fig S3

SARS-CoV-2

VSV-SARS-CoV-2-S$_{\Delta 21}$